

### 3.1.2 ATSK3\_p and ATSK3\_r

Retrieval algorithm for cloud microphysics based on a reflection method.

#### A. Algorithm Outline

- (1) Algorithm Code: ATSK3\_p, ATSK3\_r
- (2) Product Code: CLOP\_p (from ATSK3\_p)  
CLOP\_w\_r, CLER\_w\_r, CLTT\_w\_r,  
CLHT\_w\_r, CLWP\_w\_r, CLOP\_i\_r (from ATSK3\_r)

**Note:** Actually, ATSK3\_r outputs two temporary files in a day, (work\_r\_w), (work\_r\_i). The ATSK16 algorithm reads four-day's (work\_r\_w) and (work\_r\_i) and outputs products listed above.

- (3) PI names: Teruyuki NAKAJIMA
- (4) Overview of algorithm (Status: Standard level)

- Abstract

A method for satellite remote sensing of cloud microphysics has been developed to apply to ADEOS-II GLI multispectral radiance data. This algorithm is an enhanced algorithm of NOAA AVHRR data analysis (Nakajima and Nakajima 1995; Kawamoto 1999), which has an active thermal collection in absorption channel. Undesirable radiation components such as ground-reflected solar radiation and thermal radiation are guessed from satellite-received radiances in channels 13, 30 and 35 of GLI and subtracted from radiances in channels 13 and 30 to derive the reflected solar radiation of a cloud layer which includes information about cloud microphysical properties. This method can be applied to a broad range of water clouds from semi-transparent to thick clouds.

Cloud optical thickness of water and ice clouds (CLOP\_p) are retrieved by ATSK3\_p. Cloud optical thickness (CLOP\_w\_r), cloud effective particle radius (CLER\_w\_r), liquid water path (CLWP\_w\_r), cloud top temperature (CLTT\_w\_r), and cloud top height (CLHT\_w\_r) of water clouds are retrieved by ATSK3\_r. Cloud optical thickness (CLOP\_i\_r) of ice clouds are retrieved by ATSK3\_r.

- Background

Cloud feedback mechanisms are recognized as a major source of uncertainty in the current assessment of global climate change. Planetary boundary layer clouds of the marine subtropics affect the climate through coupling of radiative, microphysical and convective processes with largely different time scales (Betts and Ridgway 1989). Somerville and Remer (1984) have used a radiative-convective equilibrium model to study cloud optical thickness feedback and concluded that the sign of the feedback is negative; hence, clouds can act as a thermostat and change in such a way as to reduce the surface and tropospheric warming caused by the CO<sub>2</sub> increase. Using recent general circulation models (GCM), Roeckner et al. (1987) and Mitchell et al. (1989) also concluded that a change in cloud optical properties may result in a negative feedback comparable in size to the positive feedback associated with a change in the cloud cover. On the other hand, Wetherald and Manabe (1988) were led to a conclusion that the contribution of the negative feedback process of clouds is much smaller than the effect of the positive feedback process induced by reduced cloud amount in the upper troposphere and increased cloudiness around the tropopause. In order to improve the treatment of clouds in GCM simulations of climate change, observations of global cloud

radiative and microphysical properties are very important. The International Satellite Cloud Climatology Project (ISCCP) was initiated to develop and coordinate basic research on techniques for measuring the physical properties of clouds by satellite remote sensing and to apply the resulting techniques to derive a global cloud climatology for improving the parameterization of clouds in climate models (Schiffer and Rossow 1983).

An important possibility that increasing anthropogenic aerosols may change the cloud radiative properties has been pointed out recently by many researchers (e.g., Coakley et al. 1987; Radke et al. 1989). Twomey et al. (1984) studied the effect of anthropogenic aerosols of continental origin on the cloud albedo and concluded that the loss of sunlight may compensate for the expected warming by CO<sub>2</sub>. An interesting example of the effect of anthropogenic cloud condensation nuclei (CCN) on cloud reflectivity is the so-called *ship track* phenomenon caused by seeding of CCN from ships. Ship tracks appear frequently in satellite imagery as a signature of modification of low-lying stratus and stratocumulus clouds (Radke et al. 1989). Durkee et al. (1986) and Kaufman and Nakajima (1993) noted that the simultaneous study of both cloud and aerosol properties is important for better understanding of cloud-aerosol interaction processes.

Stimulated by the importance of cloud microphysical change problems as discussed above, there has been an increasing number of studies pertaining to the retrieval theories and methods for obtaining cloud optical thickness and particle size from multispectral radiometers on aircraft (Hansen and Pollack 1970; Twomey and Cocks 1982; King 1987; Foot 1988, Rawlins and Foot 1990; Nakajima et al. 1991) and on satellites (Curran and Wu 1982; Arking and Childs 1985; Rossow et al. 1989; Kaufman and Nakajima 1993; Platnick and Twomey 1994; Han et al. 1994, Nakajima and Nakajima 1995, Kawamoto 1999). The soundness of aircraft remote sensing retrievals of cloud microphysical properties has been extensively studied by comparisons between in situ and remote sensing-derived values. We need more effort, on the other hand, to establish the satellite remote sensing method, since there are many sources of uncertainty in the method, such as removal of undesirable radiation components in the satellite-received spectral radiance and methods of assuming the model atmosphere which we need to simulate the satellite-received radiances. There are not so many comparisons of satellite remote sensing results with in situ measurements to study these problems. There also is a room for developing techniques to improve the performance of the method. Han et al. (1994), for example, have surveyed the effective radius for near-global area by using a nadir remote sensing method, in which case the reflected radiation is independent of azimuthal angle and the effect of non-plane parallel features of clouds may be small, making use of the ISCCP CX dataset that prepares ISCCP-derived cloud optical thickness. It will be useful to study merit and demerit of off-nadir analyses.

The principal intent of this ATBD, therefore, is to introduce an efficient method for satellite remote sensing retrievals of cloud optical thickness, effective particle radius, cloud top temperature, and some related products. The present method can be applied to wide area as large in size as the view of the ADEOS-II polar orbital satellite.

## B. Theoretical Description

### (1) Methodology and Logic flow

#### ● Approach and Methodology

The ATSK3\_p (the pixel by pixel analysis corresponding GLI Level-1b area) and ATSK3\_r (the segment analysis for near-global area) uses LUT (Look up Table)-Iteration Method (LIM) to retrieve the target geophysical parameters from satellite-derived radiance data.

In the ATSK3\_r, a non-absorption channel (channel 13), an absorption channel (channel 30), and a thermal channel (channel 35) are used to derive cloud optical thickness (CLOP), cloud effective particle radius (CLER), and cloud top temperature (CLTT). Adding to these radiance data, some ancillary input data, such as the vertical profile of the temperature, pressure, water vapor, ground albedo are also used to calculate related geophysical parameters; cloud top height (CLHT) and cloud top pressure (CLTP) are retrieved by comparing cloud top temperature and temperature profile from ancillary data; liquid water path (CLWP) is calculated by cloud optical thickness and effective particle radius (Eq.9). Additional flag which identifies cirrus cloud will be output from ATSK3\_r. The cirrus flag is set by the brightness temperature difference (BDT) between channel 35 and 36 larger than 1.5 K (see ATBD of ATSK16 in detail).

On the contrary, ATSK3\_p uses only a non-absorption channel (channel 13) to retrieve cloud optical thickness (CLOP), because 3-channel LIM takes more computing time. Theoretical background and important formulas used in the ATSK3\_p and ATSK3\_r are shown in the next subsection.

#### ● Logic Flow

Basically, ATSK3\_p and ATSK3\_r is the same program. However, the calculation modes, mentioned above, can be selected by user-defined process control datafile. Four LUTs are prepared for this purpose, i. e., LUT of cloud-reflected radiance in channels 13 and 30, transmissivities and reflectivity in channels 13 and 30, channel 35 transmissivity, and the active thermal correction. Table 1 summarizes the grid system of the LUTs and Fig. 1 illustrates the flow of the analysis. We used Newton-Raphson method to iterate a main loop in the program. Some related parameters, such as; cloud geometrical thickness, liquid water path, and; cloud top height are also calculated in the algorithm with temperature slicing data from objective analysis such as JMA GANAL dataset. We found that the iteration does not converge in some cases of optically thin clouds when the removed radiation significantly dominates over the signal. In this case we cancel the analysis.

Table 1. The grid system of the look up tables;  $W_u$  and  $W_c$  are the equivalent water vapor amount of the layer of above cloud ( $w_u$ ) and cloud ( $w_c$ );  $\theta$ ,  $\theta_b$ ,  $\theta_s$  are the satellite and solar zenith angle, and relative azimuth angle.  $\tau_c$  and  $r_e$  are cloud optical thickness and effective particle radius.

<i>Quantities</i>	<i>Grid point values</i>
$W_u$	50, 5000, 10000, 20000, 30000, 40000, 50000
$W_c$	50, 5000, 10000, 20000, 30000, 40000, 50000
$\theta$ (degrees)	0, 5, 10, 20, 30, 35, 50, 45, 50, 55, 60
$\theta_b$ (degrees)	0, 5, 10, 20, 30, 35, 50, 45, 50, 55, 60, 65, 70
$\theta_s$ (degrees)	0 to 180 (divided by every 10 degrees)
$\tau_c$ (Water cloud)	1,2,4,6,9,14,12,20,30,50,70

$\overline{r}_c$ (Ice cloud)	0.1, 0.5, 1, 2, 4, 8, 16, 32, 48, 64
$r_e$ (Water cloud)	4, 6, 9, 12, 15, 20, 25, 30
$r_e$ (Ice cloud)	5, 10, 20, 40, 60, 80, 110, 140

---

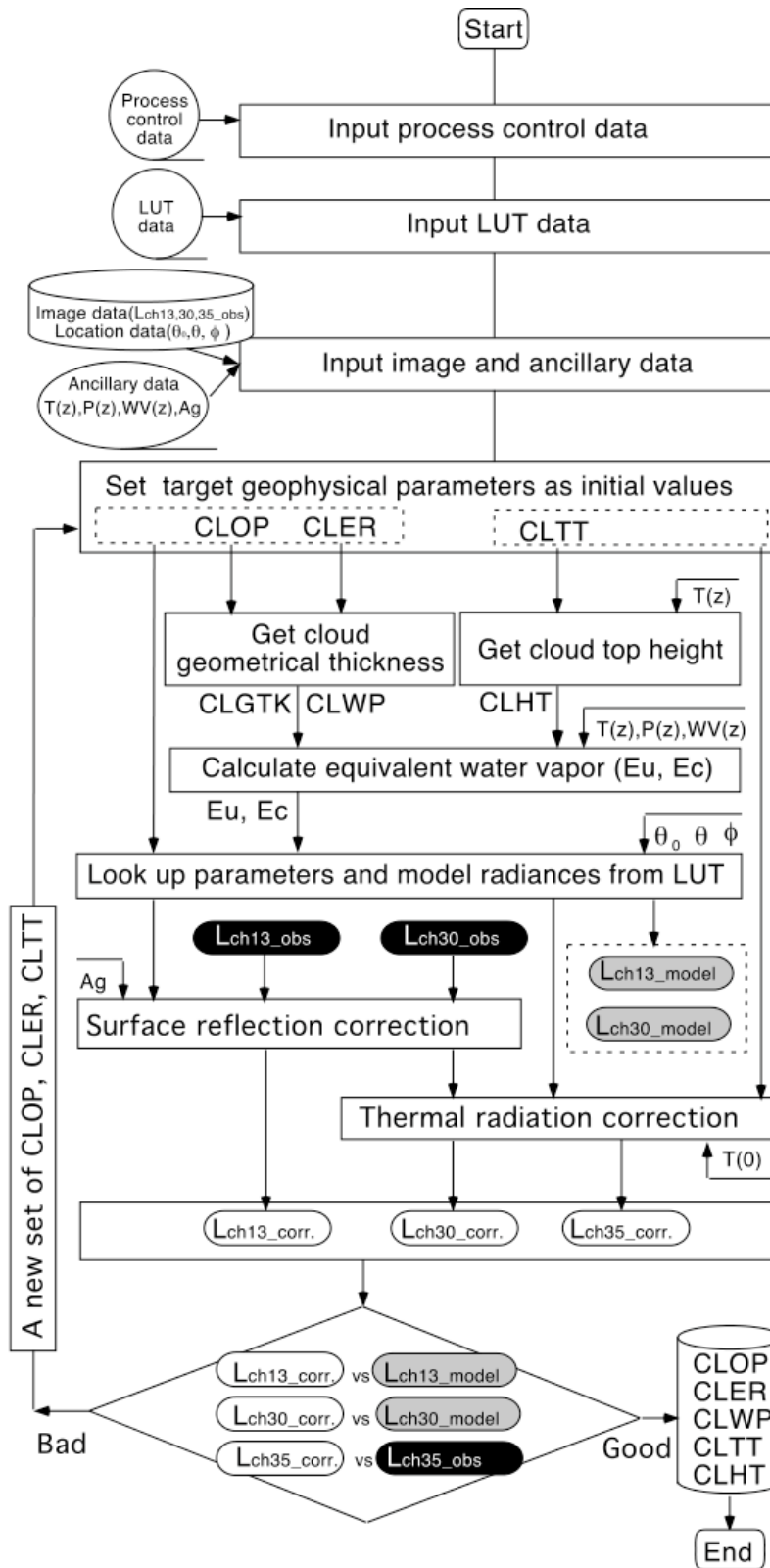


FIG. 1. Flow chart of the ATSK3\_r. In the ATSK3\_p process, only non-absorbing channel (Lch13) and ground albedo  $Ag$  are used to calculate only (CLOP\_p). Pre-process and post-process program are required to select target pixels from segment dataset and select suitable results from all outputs. Please see subsection B-(3) in this section about pre-process and post-process.

## (1) Physical and Mathematical aspects of the algorithm

## ● Concept

The solar reflectance method uses non-absorbing visible and water-absorbing near-infrared wavelengths, such as 1.6, 2.2 and 3.7  $\mu\text{m}$ , for simultaneous retrievals of cloud optical thickness and effective particle radius. In this paper we mainly discuss the solar reflectance method making use of channels 13 (0.64  $\mu\text{m}$ ), 30 (3.715  $\mu\text{m}$ ) and 35 (10.8  $\mu\text{m}$ ) of GLI aboard ADEOS-II polar orbiter. Figure 2 illustrates a simulation of reflected solar radiances in channels 13 and 30 of GLI as a function of the cloud optical thickness ( $\tau_c$ ) and effective cloud particle radius ( $r_e$ ) as defined by

$$r_e = \frac{\int_0^\infty r^3 n(r) dr}{\int_0^\infty r^2 n(r) dr}, \quad (1)$$

where  $n(r)$  is the number size distribution as a function of particle radius  $r$ . We used a log-normal size distribution in the calculation,

$$n(r) = \frac{N}{\sqrt{2\pi}\sigma} \exp\left[-\frac{(\ln r - \ln r_0)^2}{2\sigma^2}\right], \quad (2)$$

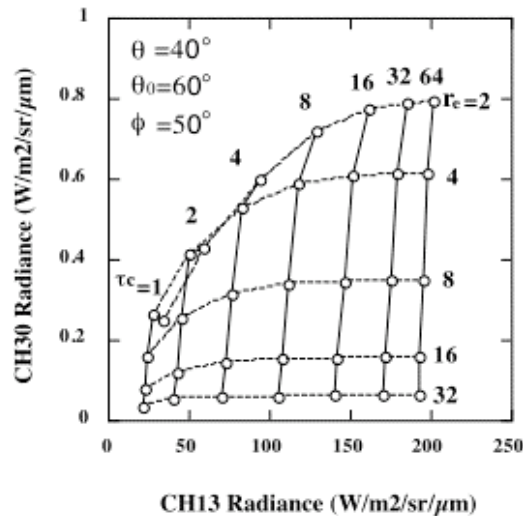


FIG. 2. Simulation of reflected solar radiances in GLI channels 13 and 30 as a function of cloud optical thickness ( $\tau_c=1, 2, 4, 8, 16, 32$  and  $64$ ) and effective radius ( $r_e=2, 4, 8, 16$  and  $32$ ) with the condition of  $\theta=40^\circ$ ,  $\theta_0=60^\circ$  and  $\phi=60^\circ$ . Near-vertical and near-horizontal lines illustrate iso-optical thickness and iso-effective radius radiances, respectively. Ground-reflected and thermal radiations are not taken into account in this result. LOWTRAN-7 and U. S. Standard model were assumed to model gaseous absorption.

where  $r_0$  is the mode radius, which is related to the effective radius as  $r_e = r_0 e^{3.5\sigma^2}$ , and  $\sigma$  is the log-standard deviation of the size distribution.  $\sigma = 0.35$  was assumed for marine stratocumulus clouds in our analyses. For the satellite signal simulation, we used an accurate and efficient radiative transfer scheme (Nakajima and Tanaka, 1986, 1988; Nakajima and King, 1992) extended to include thermal radiative transfer as

proposed by Stamnes et al. (1988). In the radiative transfer calculation we used the  $k$ -distribution of absorption coefficient from LOWTRAN-7 (Kneizys et al., 1988) for a gas absorption model. The Midlatitude Summer atmosphere model was divided into four plane-parallel layers with interfaces at 1, 2 and 12 km and the top at 120 km in this example. The cloud is inserted into the third layer from the top of the model atmosphere with saturated humidity in the cloud layer. As for the underlying surface, we assumed a Lambert surface. This assumption will not introduce a significant error in the analyses if we use an equivalent flux albedo as suggested by Nakajima et al. (1991) for cloudy atmospheres.

We recognize in Fig. 1 that the reflected solar radiance in channel 13, 30 primarily depends on the cloud optical thickness whereas the reflected radiance in channel 30 primarily depends on the effective radius. This fact can be explained by the difference in the magnitude of the imaginary index of refraction of liquid water in channel 13 ( $\sim 10^{-9}$ ) and channel 30 ( $\sim 10^{-3}$ ). Since the solar radiation in channel 13 penetrates more deeply into the cloud layer than that in channel 30, larger optical thicknesses ( $\sim 100$ ) can be retrieved from channel 13 radiance than optical thicknesses ( $\sim 10$ ) from channel 30. The moderately large imaginary index of refraction in channel 30 makes the radiance sensitive to particle size. The sensitivity is larger than those of  $1.6 \mu\text{m}$  or  $2.2 \mu\text{m}$  at which measured radiances do not include thermal radiation. In channel 30, instead, we have to take into account the effect of thermal radiation as discussed in the following subsection.

As  $\tau_c$  and  $r_e$  decrease, multiple solutions of  $\tau_c$  and  $r_e$  are possible as noted by Nakajima and King (1990). The reason for this phenomenon is that the optical thickness in channel 30 takes the maximum value at  $r_e \sim 4 \mu\text{m}$  when the optical thickness in channel 13 is fixed constant. When the cloud is optically thin, the ratio of channel 30 radiance to channel 13 radiance (i. e., the slope of iso-effective radius lines in FIG. 2) becomes a good index of particle size. Wielicki et al. (1990) used those slopes at  $1.6$  and  $2.2 \mu\text{m}$  Bands of LANDSAT TM for cirrus-particle sizing.

### 1. Removal of undesirable radiation components

Although the concept of the retrieval is simple, some difficulties will occur when we determine the cloud microphysical properties from measured spectral radiances of GLI. We have to decouple the radiation reflected by the cloud layer, which depends on cloud optical thickness and particle size, from other undesirable radiation components, such as solar radiation reflected by the ground surface, especially for optically thin clouds, and thermal radiation emitted from cloud layer and ground surface in channel 30. Figures 2 and 3 illustrate simulated radiances ( $\text{W m}^{-2} \text{sr}^{-1} \mu\text{m}^{-1}$ ) in channels 13 and 30 as a function of cloud optical thickness  $\tau_c$  and ground surface albedo  $A_g$ . Similar figures were presented by King (1987) at wavelengths of  $0.75 \mu\text{m}$  and  $1.63 \mu\text{m}$ . We see, in these figures, that ground reflectance largely contributes to the satellite signal in the full range of  $\tau_c$  in channel 13 whereas it becomes important only for  $\tau_c$  less than 10 in channel 30.

Figure 5 illustrates simulated radiances in channel 30 as a function of  $\tau_c$  in cases containing 1) no thermal radiation, 2) ground thermal radiation, 3) cloud thermal radiation, and 4) both ground and cloud thermal radiation. In this simulation, the surface albedo  $A_g$ , ground  $T_g$  and cloud temperatures  $T_c$  are set to  $=0.0$ ,  $=288.2 \text{ K}$  and  $=275.2 \text{ K}$ , respectively. This figure indicates that the radiance in channel 30 is influenced by the ground thermal radiation in the range of  $\tau_c < 10$ , whereas it is affected

by the cloud thermal radiation in the range of  $\tau_c > 2$ . Even for optically thin clouds ( $\tau_c < 2$ ), we can see an effect of thermal radiation.

These undesirable radiation components have to be removed from the measured radiances. Rossow (1989) noted that the success of this kind of analysis depends on the fidelity of the radiative transfer model used in the data analyses and the accuracy of specifying the other properties of atmosphere and ground surface that affect the measured radiance. Kaufman and Nakajima (1993) have adopted a simple method of subtracting thermal radiation by using an effective temperature derived from channel 35 and the optical thickness guessed from channel 13, by which we can calculate the cloud reflectivity in channel 30 without thermal radiation. Of course, this approximation is adequate for optically thick clouds because their neglected small transmissivity prevents ground-reflected radiation and ground thermal radiation transmitting to the space. King and Harshvardhan (1986) noted that the transmissivity of cloud layers can be neglected for  $\tau_c > 10$ . As an alternative method, thermal radiation in channel 30 has been determined from radiance in channel 35 that is fitted as a function of radiance in channel 30 using night time measurements (Coakley and Davies, 1986). A ground-reflected radiation and ground thermal radiation, however, are not so small as to neglect for optically thin clouds. Also, the fitting method does not handle well dual-source thermal

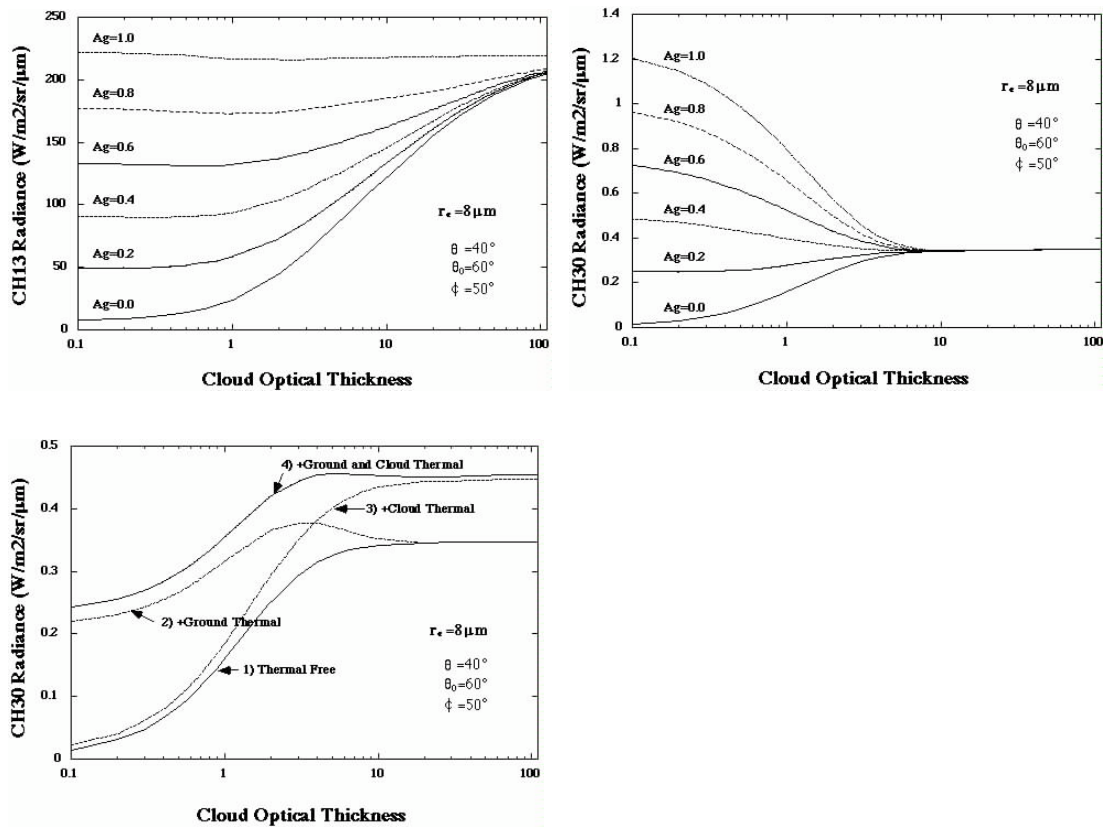


FIG. 3 (Upper left) Simulated radiances in channel 13 ( $0.678 \mu\text{m}$ ) as a function of cloud optical thickness and ground surface albedo under the same condition as in FIG. 2. The effective particle radius is fixed at  $8 \mu\text{m}$ .

FIG. 4 (Upper right) As in FIG. 3 except for channel 30 ( $3.715 \mu\text{m}$ ).

FIG. 5. (Lower left) Simulated thermal emission contributions in channel 30 under the same condition as in FIG. 2.

radiation that is frequently observed when clouds are optically thin.

Thus, it will be very useful to find an effective method to infer the cloud reflectivity by decoupling it from the undesirable radiation components by making explicit use of radiative transfer theory and all of the information of channels 13, 30 and 35. Ou et al. (1993) developed such a method for their cirrus cloud retrievals, but they used the thermal radiation information for their purpose by subtracting the reflected radiation from the satellite-received radiances.

## 2. Expression of the radiation components

According to the radiative transfer theory for plane parallel layers with an underlying Lambert surface, we can decouple the radiance reflected by the cloud layer,  $L$ , from the satellite-received radiance,  $L_{obs}$ , by removing the undesirable radiance components as follows:

for visible wavelength ( $0.678\mu\text{m}$ , channel 13),

$$L(w_u, w_c, \mu, r_e; \mu_0, \mu_s) = L_{obs}(w_u, w_c, \mu, r_e; \mu_0, \mu_s) - t(w_u, w_c, \mu, r_e; \mu_0) \frac{A_g}{1 - \bar{r}(w_u, w_c, \mu, r_e) A_g} \frac{\mu_0 F_0}{\mu}, \quad (3)$$

and for near-infrared wavelength ( $3.715\mu\text{m}$ , channel 30),

$$\begin{aligned} L(w_u, w_c, \mu, r_e; \mu_0, \mu_s) &= L_{obs}(w_u, w_c, \mu, r_e; \mu_0, \mu_s) \\ &- t(w_u, \mu_u, \mu) [1 - t(w_c, \mu_c, r_e; \mu) - r(w_c, \mu_c, r_e; \mu)] B(T_c) \\ &- t(w_u, w_c, \mu, r_e; \mu) \frac{1 - A_g}{1 - \bar{r}(w_u, w_c, \mu, r_e) A_g} B(T_g) \\ &- t(w_u, w_c, \mu, r_e; \mu) \frac{A_g}{1 - \bar{r}(w_u, w_c, \mu, r_e) A_g} t(w_u, w_c, \mu, r_e; \mu_0) \frac{\mu_0 F_0}{\mu} \\ &- L_{ml}(w_u, T_c) \\ &- t(w_u, \mu_u, \mu) t(w_c, \mu_c, r_e; \mu) L_{ml}(w_d, T_g) \end{aligned}, \quad (4)$$

where  $F_0$  is the extraterrestrial solar flux and  $B$  is the Planck function;  $\mu$ ,  $\mu_c$  and  $\mu_u$  are respectively the optical thicknesses of atmosphere, cloud layer and the atmosphere above the cloud layer;  $\mu_0$  and  $\mu_s$  are respectively the cosines of solar and satellite zenith angles, and  $\phi$  is the azimuthal angle of the satellite relative to the sun.  $w_u$ ,  $w_c$ , and  $w_d$  are the equivalent water vapor amount, which is defined as

$$w_{u,c,d} = \int_{z_l}^{z_2} w(z) \left[ \frac{P(z)}{P_g} \right]^{0.5} \left[ \frac{T_g}{T(z)} \right]^{0.9} dz \quad (5)$$

where,  $z_l$  and  $z_2$  are, ground level and cloud bottom, cloud bottom and cloud top, cloud top and top of atmosphere, for the case of  $w_u$ ,  $w_c$ , and  $w_d$ .  $P(z)$  and  $T(z)$  are the vertical profile of the air pressure and air temperature as a function of altitude  $z$ ,  $P_g$  and  $T_g$  is the surface pressure and temperature.

The transmissivity  $t$ , plane albedo  $r$  and spherical albedo  $\bar{r}$  are given by,

$$t(w_u, w_c, \mu, r_e; \mu_0) = \frac{1}{\mu} \int_0^{2\pi} \int_0^1 T(w_u, w_c, \mu, r_e; \mu, \mu_0, \mu_s) d\phi d\mu_s + e^{-\mu/\mu_0}, \quad (6)$$

$$r(w_u, w_c, \bar{\rho}, r_e; \bar{\rho}) = \frac{1}{\bar{\rho}} \int_0^{2\bar{\rho}} \int_0^1 R(w_u, w_c, \bar{\rho}, r_e; \bar{\rho}, \bar{\rho}) d\bar{\rho} d\bar{\rho}, \quad (7)$$

and

$$\bar{r}(w_u, w_c, \bar{\rho}, r_e) = 2 \int_0^1 T(w_u, w_c, \bar{\rho}, r_e; \bar{\rho}) d\bar{\rho}, \quad (8)$$

where  $T(w_u, w_c, \bar{\rho}, r_e; \bar{\rho}, \bar{\rho})$  and  $R(w_u, w_c, \bar{\rho}, r_e; \bar{\rho}, \bar{\rho})$  are bi-directional transmission and reflection functions respectively. The second term of Eq. (3) and the fourth term of Eq. (4) are ground-reflected radiation components, the second and third terms of Eq. (4) are cloud and ground thermal radiation components. The fourth and fifth terms of Eq. (4) are active thermal correction components from the layer of above the cloud, and below the cloud respectively. These quantities are parameterized by  $w_u T_c^{1.5}$ .

Multiple reflection between ground surface and the upper layer is taken into consideration in Eqs. (3) and (4). This effect is very small, however, enough to regard  $\bar{r}(w_u, w_c, \bar{\rho}, r_e) A_g$  as almost zero, especially for an optically thin cloud and for ground surface of low reflectance. On the contrary, with optically thick cloud and large ground albedo, this effect is relatively large at visible wavelength because the large cloud spherical albedo reflects radiation from the ground surface and the relatively large transmissivity allows this radiation component transmitting to the space.

These formulations are exact apart from the neglected thermal radiation from the atmosphere other than the cloud layer, when we treat monochromatic radiances. We further introduce a wavelength averaging of variables in the formulations. For example,  $t$  is averaged with sub-channel response function of GLI as,

$$t = \frac{\sum_{n=1}^N \bar{\rho}_n \sum_{k=1}^M (\bar{\rho}_{n,k} t_{n,k})}{\sum_{v=1}^n \bar{\rho}_v}, \quad (10)$$

where  $\bar{\rho}_n$  is the response function of  $n$ th subchannel wavelength for each GLI channel (We used  $\bar{\rho}_n$  values obtained from <http://www.eorc.nasda.go.jp/ADEOS-II/GLI/index.html>);  $\bar{\rho}_{n,k}$  is the weight of  $k$ th  $k$ -distribution and  $t_{n,k}$  is transmissivity for the  $k$ th  $k$ -distribution at  $n$ th wavelength. In the calculation,  $n$  is 22 for channel 13 and 35, 21 for channel 30, and  $k$  is 3. This averaging, applied to Eqs. (3) and (4), brings a non-negligible error in the case of thin cloud layers in which spectral variation of  $t_{n,k}$  becomes large. However, for most cases of our application, the error remains small and we can estimate undesirable radiation components in Eqs. (3) and (4) with variables spectrally averaged for each channel.

### 3. Liquid water path calculated from optical thickness and effective radius.

The liquid water path is calculated by

$$W = \frac{2\bar{\rho}_c r_e}{3}. \quad (11)$$

## (2) Pre-process and post-process of ATSK3\_r.

The ATSK3\_r analyses atmospheric segment data. The atmospheric segment data has 25 pixels in one segment (0.25 x 0.25 degrees square area), and not all pixels will be identified to clouds in most cases. Therefore, the ATSK3\_r needs pre-process program which choose target pixels analyzed by ATSK3\_r and post-process which calculates statistic values from four-day output (work\_r\_w and work\_r\_I) of ATSK3\_r.

Two options are available when the pre-process program of ATSK3\_r chooses target cloud pixel(s) from one segment. One is method which choose one "suitable" pixel from 25 pixels in one segment (we call this method "*saving-time method*"), the other method choose all pixels in one segment that are identified cloud referring (CLFLG) obtained by ATSK1+2 algorithm (see ATBD of ATSK1+2 in detail) (we call this method "*full-specification method*"). Median selection, mode selection, and maximum selection, of non-absorption channel (channel 13) can be selected to obtain "suitable" one from 25 pixels. If *saving-time method* is chosen, the post-process program of ATSK3\_r (that is ATSK16) simply averages four-day output (work\_r\_w and work\_r\_I) of every segment. If *full-specification method* is chosen, ATSK16 simply averages four-day output (work\_r\_w and work\_r\_I) of every segment for rough-classification, and classify all output from one segment into 11 cloud types in order to obtain cloud fraction (CLFR) for detailed-classification (see ATBD of ATSK16 in detail). The normal operation of ATSK3\_r, we will choose *full-specification method*. However, during the checkout period for GLI project, *saving-time method* with mode selection option will be chosen to check the optical performance of GLI sensor, and computing performance of data analysis system.

### C. Practical Considerations

## (1) Programming, Procedural, Running Considerations

Program Requirements: The following table shows information about the expected software generated from this algorithm.

Program Memory	53.9 MBytes
Program Size	3509 lines
Required Channels	Channel 13, 30, 35
Necessary/Ancillary Data	Objective Analysis data, Look up tables
Expected Disk Volume	221.4 MBytes
Special Programs or Subroutines	Pre-process and post-process program are required to select target pixels from Level-1B or segment dataset, and select suitable results from all outputs.

## (2) Calibration and validation

*Under construction.*

## (3) Quality Control and Diagnostic Information

*Under construction.*

## (4) Exception Handling

*Under construction.*

## (5) Constraints, Limitations, Assumptions

*Under construction.*

## (6) Publications and Papers

Nakajima, T. Y. and T. Nakajima, 1995: Wide-area determination of cloud

microphysical properties from NOAA AVHRR measurements for FIRE and ASTEX regions. *J. Atmos. Sci.*, **52**, 4043-4059

Kawamoto, K. 1999: On the global distribution of the water cloud microphysics derived from AVHRR remote sensing, Ph.D. dissertation University of Tokyo, Tokyo, Japan.

Kawamoto, K., T. Nakajima, and T. Y. Nakajima, 1999: A global determination of cloud microphysics with AVHRR remote sensing. *J. Climate*, Submitted.

## D. References

- Arking, A., and J. D. Childs, 1985: Retrieval of cloud cover parameters from multispectral satellite images. *J. Clim. Appl. Meteor.*, **24**, 322-333.
- Betts, A. K., and W. Ridgway, 1989: Climatic equilibrium of the atmospheric convective boundary layer over a tropical ocean. *J. Atmos. Sci.*, **46**, 2621-2641.
- Coakley, J. A., Jr., and R. Davies, 1986: The effect of cloud sides on reflected solar radiation as deduced from satellite observations. *J. Atmos. Sci.*, **43**, 1025-1035.
- Coakley, J. A., Jr., R. L. Bernstein and P. A. Durkee, 1987: Effect of ship-stack effluents on cloud reflectivity. *Science*, **237**, 1020-1022.
- Curran, R. J., and M. L. C. Wu, 1982: Skylab near-infrared observations of clouds indicating supercooled liquid water droplets. *J. Atmos. Sci.*, **39**, 635-647.
- Durkee, P. A., D. R. Jensen, E. E. Hindman and T. H. V. Haar, 1986: The relationship between marine aerosol particles and satellite detected radiance. *J. Geophys. Res.*, **91**, 4063-4072.
- Foot, J. S., 1988: Some observations of the optical properties of clouds. I: Stratocumulus. *Quart. J. R. Met. Soc.*, **114**, 129-144.
- Han, Q., W. B. Rossow and A. A. Lacis, 1994: Near-Global survey of effective droplet radii in liquid water clouds using ISCCP data. *J. Climate*, **7**, 465-497.
- Hansen, J. E., and J. B. Pollack, 1970: Near-infrared light scattering by terrestrial clouds. *J. Atmos. Sci.*, **27**, 265-281.
- Kaufman, Y. J., and T. Nakajima, 1993: Effect of amazon smoke on cloud microphysics and albedo - Analysis from satellite imagery. *J. Appl. Meteor.*, **32**, 729-744.
- King, M. D., and Harshvardhan, 1986: Comparative accuracy of the albedo, transmission and absorption for selected radiative transfer approximations. NASA Reference Publication, 1160, 41 pp.
- King, M. D., 1987: Determination of the scaled optical thickness of clouds from reflected solar radiation measurements. *J. Atmos. Sci.*, **44**, 1734-1751.
- Kneizys, F. X., E. P. Shettle, L. W. Arbeau, J. H. Chetwynd, G. P. Anderson, W. O. Gallery, J. E. A. Selby, and S. A. Clough, 1988: Users guide to LOWTRAN-7. AFGL-TR-88-0177, 137 pp.
- Mitchell, J. F. B., C. A. Senior and W. J. Ingram, 1989: CO<sub>2</sub> and climate: A missing feedback? *Nature*, **341**, 132-134.
- Nakajima, T., and M. Tanaka, 1986: Matrix formulation for the transfer of solar radiation in a plane-parallel scattering atmosphere. *J. Quant. Spectrosc. Radiat. Transfer*, **35**, 13-21.
- Nakajima, T., and M. Tanaka, 1988: Algorithms for radiative intensity calculations in moderately thick atmospheres using a truncation approximation. *J. Quant. Spectrosc. Radiat. Transfer*, **40**, 51-69.

- Nakajima, T., and M. D. King, 1990: Determination of the optical thickness and effective radius of clouds from reflected solar radiation measurements. Part I: Theory. *J. Atmos. Sci.*, **47**, 1878-1893.
- Nakajima, T., and M. D. King, 1992: Asymptotic theory for optically thick layers: Application to the discrete ordinates method. *Appl. Opt.*, **31**, 7669-7683.
- Nakajima, T., M. D. King, J. D. Spinhirne, and L. F. Radke, 1991: Determination of the optical thickness and effective radius of clouds from reflected solar radiation measurements. Part II: Marine stratocumulus observations. *J. Atmos. Sci.*, **48**, 728-750.
- Ou, S. C., K. N. Liou, W. M. Gooch, and Y. Takano, 1993: Remote sensing of cirrus cloud parameters using advanced very-high-resolution radiometer 3.7- and 10.9- $\mu\text{m}$  channels. *Appl. Opt.*, **32**, 2171-2180.
- Platnick, S. and S. Twomey, 1994: Determining the susceptibility of cloud albedo to changes in droplet concentration with the Advanced Very High Resolution Radiometer. *J. Appl. Meteor.*, **33**, 334-347.
- Radke, L. F., J. A. Coakley, Jr., and M. D. King, 1989: Direct and remote sensing observations of the effect of ships on clouds. *Science*, **246**, 1146-1149.
- Rawlins, F., and J. S. Foot, 1990: Remotely sensed measurements of stratocumulus properties during FIRE using the C130 aircraft multi-channel radiometer. *J. Atmos. Sci.*, **47**, 2488-2503.
- Roeckner, E., U. Schlese, J. Biercamp and P. Loewe, 1987: Cloud optical depth feedbacks and climate modelling. *Nature*, **329**, 138-140.
- Rossow, W. B., 1989: Measuring Cloud Properties from Space: A Review. *J. Climate*, **2**, 201-213.
- Rossow, W. B., L. C. Garder and A. A. Lacis, 1989: Global, seasonal cloud variations from satellite radiance measurements. Part I: Sensitivity of analysis. *J. Climate*, **2**, 419-458.
- Schiffer, R. A., and W. B. Rossow, 1983: The International Satellite Cloud Climatology Project (ISCCP): The first project of the World Climate Research Programme. *Bull. Amer. Meteor. Soc.*, **64**, 779-784.
- Somerville, R. C. J., and L. A. Remer, 1984: Cloud optical thickness feedbacks in the CO<sub>2</sub> climate problem. *J. Geophys. Res.*, **89**, 9668-9672.
- Stamnes, K., S.-C. Tsay, W. Wiscombe, and K. Jayaweera, 1988: Numerically stable algorithm for discrete-ordinate-method radiative transfer in multiple scattering and emitting layered media. *Appl. Opt.*, **27**, 2502-2509.
- Twomey, S., and T. Cocks, 1982: Spectral reflectance of clouds in the near-infrared: Comparison of measurements and calculations. *J. Meteor. Soc. Japan*, **60**, 583-592.
- Twomey, S., M. Piepgrass and T. L. Wolfe, 1984: An assessment of the impact of pollution on global cloud albedo. *Tellus*, **36**, 356-366.
- Twomey, S., and T. Cocks, 1989: Remote sensing of cloud parameters from spectral reflectance in the near-infrared. *Beitr. Phys. Atmos.*, **62**, 172-179.
- Wetherald, R. T., and S. Manabe, 1988: Cloud feedback processes in a general Circulation model. *J. Atmos. Sci.*, **45**, 1397-1415.
- Wielicki, B. A., J. T. Suttles, A. J. Heymsfield, R. M. Welch, J. D. Spinhirne, M.-L. C. Wu, D. O'C. Starr, L. Parker, and R. F. Arduini, 1990: The 27-28 October FIRE IFO Cirrus Case Study: Comparison of radiative transfer theory with observations by satellite and aircraft. *Month. Weath. Rev.*, **118**, 2356-2376.